Texture Feature Coding Method for Texture Segmentation and Classification

Abstract

This paper proposes a new texture analysis method namely texture feature coding method (TFCM). The texture feature coding method transforms a gray-level image into feature image whose each pixel is represented by a texture feature number (TFN). The TFN histogram and TFN co-occurrence matrix are derived to generate many texture features for texture classification. The gray-level co-occurrence matrix (GLCM) and texture spectrum (TS) have been used for comparison in discriminating some of Brodatz's natural texture images and ultrasonic liver images in experiments.

Experimental results reveal that the results using the texture feature coding methods is superior to other two.

Keywords: Texture analysis, Texture feature coding method, Gray-level co-occurrence matrix, Texture spectrum

1. Introduction

Texture analysis is an important technique in many applications of analysis for classification or segmentation of image. In the texture segmentation, the pixels are grouped together to form regions of uniform texture based on the distribution of local

features, whereas in the texture classification, the problem is to classify an instance of a textured region in an image as one of a set of classes. The general methods for feature extraction are estimate the local textures at each pixel in a texture images and thus derive a set of statistics from the distributions of the local features. There are several methods for defining the textural features. Each method has its own way to define the features that are used in the classification problem. In the practice, structural and statistical approaches are the two major methods for extracting texture features. In the structural methods, texture is regarded as the repetition of some basic primitive patterns with a certain rule of placement. The Fourier spectrum analysis [1] is a well-known method for determining the primitive and the displacement rule. In the statistical method, texture is considered as the distribution of texture features that are extracted on a local area on the textural image. The gray-level co-occurrence matrix (GLCM) [2] and texture spectrum (TS) [3] are two widely used texture analysis methods in the category.

In this paper, we propose a new texture analysis method called texture feature coding method. It is used to analyze the Brodatz's texture images and ultrasonic liver images for classification.

This paper is organized as follows. In section 2 we describe the two methods. In section 3 of this paper we propose a new texture analysis method namely texture feature coding method (TFCM) that contains the advantages of both the GLCM and TS of texture analysis. Section 4 discusses the performance of TFCM with the GLCM and TS method by testing some of Brodatz's natural texture images. Finally, the conclusion of this paper is given.

2. Previous Works

GLCM and TS methods of texture analysis are briefly described here. Techniques of both methods are utilized in the development of the TFCM method.

2. 1 Gray-Level Co-occurrence Matrix [1]

A co-occurrence matrix is generally referred to as a gray-level co-occurrence matrix whose entries are transitions between all pairs of two gray levels (not necessarily distinct) [1]. The gray-level transitions are calculated based on two parameters, displacement d and angular orientation θ. More precisely, let i and j be two gray levels and $N_{d,\theta}(i,j)$ denote the number of transitions between two pixels whose gray levels are i and j with d-pixels apart and angular orientation θ. In other words, $N_{d,\theta}(i,j)$ is the number of pixel-pairs at locations (x, y) and (w, z) satisfying the following conditions;

$$G(x,y)=i, G(w,z)=j, \|(x,y)-(w,z)\|_{dm}=(d,\theta)$$

where $\|(x,y)-(w,z)\|_{dm}=(d,\theta)$ is a distance measure

to describe the distance between two pixels of spatial locations at (x, y) and (w, z) with d-pixels apart and along angular orientation θ. Normalizing $N_{d,\theta}(i,j)$ yields the probability or the relative frequency of gray-level transitions.

$$p(i,j|d,\theta)=\frac{N_{d,\theta}(i,j)}{N} \qquad (1)$$

Where N is the number of total gray-level transitions in the co-occurrence matrix.

Based on the gray-level co-occurrence matrix, Haralick [1] proposed 13 feature measures for texture analysis under a specific d-pixels apart and angular orientation θ. There are angular second moment, correlation, variance, inverse difference moment, entropy, sum entropy, difference entropy, information measure of correlation, sum average, contrast, sum variance, difference variance. Because of the descriptive and easily computable nature, the co-occurrence features have been widely used in most of the texture analysis problems.

2. 2 Texture Spectrum [3]

The texture spectrum was first proposed by He and Wang in [3]. The idea is to consider a so-called texture unit described by Fig. 1 with V_0, the central pixel, designated as the pixel currently examined and its 8 neighboring pixels $V_i, i > 0$. Three values $\{0,1,2\}$ will be assigned to V_i respectively according to $V_i < V_0$, $V_i = V_0$, $V_i > V_0$ as given below.

In equation (2), the Δ is denoted to tolerance of variation. Obviously, there are $3^8 = 6561$ combinations for the E_i in equation (2). The distribution of occurrence of all texture numbers N_{E_i} generated by equation (2) is called texture spectrum. As the texture unit represents the local texture information of a given pixel and its neighborhood, the statistics of all the texture units in an image reveal its global texture aspects. Several features are useful for classification and defined in [3], being,

V_2	V_3	V_4
V_1	V_0	V_5
V_8	V_7	V_6

Figure 1. 3x3 texture unit of texture spectrum

$$E_i = \begin{cases} 0 & \text{if } V_i - V_0 < \Delta \\ 1 & \text{if } V_i = V_0 \\ 2 & \text{if } V_i - V_0 > \Delta \end{cases} \quad \text{where} \quad (2)$$

V_0 = the gray level of the central pixel.

$$N_{E_i} = \sum_{j=1}^{8} V_j \cdot 3^{j-1}$$

black-white symmetry (BWS), geometric symmetry (GS), degree of direction (DD), orientation features (MHS, MVS, MDS1 and MDS2) and central symmetry (CS).

3. Texture Feature Coding Method

In this section, we propose a novel approach to generating texture feature numbers, called **T**exture **F**eature **C**oding **M**ethod (TFCM). The design rationale of this method is based on gray-level variations of a 3×3 texture unit.

3. 1 Texture Feature Number Generation

TFCM is a coding scheme, which transforms an original image into a texture feature image whose pixels are represented by texture feature numbers. The texture feature number of each pixel **X** is generated on the basis of gray-level changes of its 8 surrounding pixels, called a texture unit, a term was used in He and Wang's work [3] described in Fig. 1.

2	1	2
1	X	1
2	1	2

Fig. 2. 3x3 texture unit of TFCM

Unlike He and Wang's texture spectrum, we consider the connectivity of the texture unit. The 8 neighboring pixels in Fig. 2 constitute the 8-connectivity of the texture unit, which can be divided into the first-order 4-connectivity pixels and second-order 4-connectivity pixels. The four pixels labeled **1** satisfy the first-order 4-connectivity of the texture unit because they are immediately adjacent to the pixel **X**. They will be denoted by first-order connectivity pixels. The other four pixels labeled **2** satisfy the second-order 4-connectivity of the texture unit, which are diagonally adjacent to **X** and will be denoted by second-order connectivity pixels. In order to code pixel **X** in Fig. 2, TFCM produces a pair of integers (r, s) where r and s represent gray-level variations of first-order connectivity and second-order connectivity respectively. As shown in Fig. 3, two scan lines along the 0°-180° and 90°-270°

directions produce two sets of three successive first-order connectivity with pixel **X** in the middle of the horizontal and vertical lines forming by "+". Similarly, two scan lines along the diagonal directions 45°-225° and 135°-315° forming by " $\mathbf{I}$ " also produce two sets of three successive second-order connectivity pixels as shown in Fig. 4.

2	1	2
1	X	1
2	1	2

+: 0°-180° scan line
90°-270° scan line

Fig. 3. First-order 4-connectivity

2	1	2
1	X	1
2	1	2

$\times$: 45°-225° scan line
135°-315° scan line
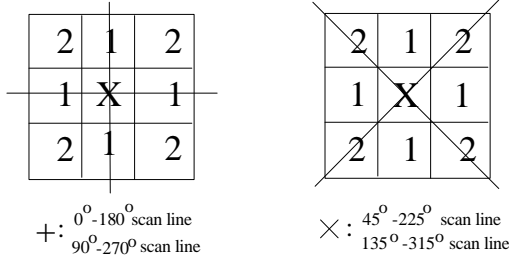
Fig. 4. Second-order 4-connectivity

Assume that the scan direction is from top to down and left to right, the three successive pixels can be arranged as *(a, b, c)* in the scanning order. For example, if *(a, b, c)* represents pixels scanned by the vertical line of the first-order connectivity in Fig. 3, the top pixel is denoted by *a*, pixel X by *b* and the bottom pixel by *c*. Suppose that (G_a, G_b, G_c) corresponds the gray levels of three pixels (*a*, *b*, *c*) respectively. If we consider two successive gray-level changes between two pairs (G_a, G_b) and (G_b, G_c), there are four different types of variations. The four types of gray-level variation defined by equation (3) can be graphed by the gray-level graphical structure shown in Fig. 5. Type (i) describes the case that the gray levels of *a, b* and *c* are very close within the tolerance Δ. Type (ii) is the case that one pair of gray levels is within Δ, but the gray-level variation of the other pair variation exceeds Δ. Type (iii) is the case where the gray levels of *a*, *b*, *c* are continuously decreasing or increasing with gray-level differences larger than Δ. In Type (iv), the gray-level variation is first decreasing then increasing or first increasing then decreasing which the increments and decrements exceed Δ.
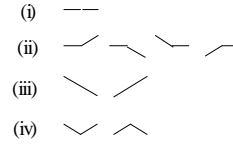
(i) ――
(ii) ⟋ ⟍ ⟍ ⟋
(iii) ⟍ ⟋
(iv) ⌄ ⌃

Fig. 5. Types of gray-level graphical structure variations

(i) $if\ (\left|G_a - G_b\right| \leq \Delta) \cap (\left|G_b - G_c\right| \leq \Delta)$

(ii) $if\ [(\left|G_a - G_b\right| \leq \Delta) \cap (\left|G_b - G_c\right| \geq \Delta)]$
$\cup [(\left|G_a - G_b\right| \geq \Delta) \cap (\left|G_b - G_c\right| \leq \Delta)]$ (3)

(iii) $if\ [(G_a - G_b > \Delta) \cap (G_b - G_c > \Delta)]$
$\cup [(G_b - G_a > \Delta) \cap (G_c - G_b > \Delta)]$

(iv) $if\ [(G_a - G_b > \Delta) \cap (G_c - G_b > \Delta)]$
$\cup [(G_b - G_a > \Delta) \cap (G_b - G_c > \Delta)]$

According to this definition of gray-level graphical structure variation. The higher the type number is, the greater gray-level variation will occur. Since both r and s, corresponding to first and second order connectivity respectively, have two scan lines, each of which can produce a type of gray-level variation, r and s can be assigned by a pair of gray-level graphical structure variations. The total number of combinations of arbitrary two gray-level graphical structure variations (including self combinations) is $\frac{4(4+1)}{2} = 10$. The 10 combinations are listed in Fig.6.

Scan line1

		(i)	(ii)	(iii)	(iv)
Scan	(i)	1	2	3	5
line2	(ii)	2	7	11	13
	(iii)	3	11	17	19
	(iv)	5	13	19	23

Fig. 6. The variation generation of first-order (r) or second-order (s) 4-connectivity

For example, if r or $s = 11$, there is a combination of (ii) and (iii). More precisely the columns represent the horizontal scan line 0°-180° for r or the diagonal line 45°-225° for s, and the rows represent the

vertical scan line 90°-270° for r or the asymmetric diagonal line 135°-315° for s. Finally, the texture feature number of each pixel is generated by taking the product of r and s. Let the gray level of the pixel with spatial location (x, y) be denoted by $G(x, y)$ and the corresponding texture feature number by $TFN(x, y)$. Then

$$TFN(x, y) = r(x, y) \times s(x, y) \qquad (4)$$

where $r(x, y)$ and $s(x, y)$ are values obtained using Fig. 6 for the pixel at spatial location (x, y).

3.2 Texture Feature Number Histogram and Texture Feature Number Co-occurrence Matrix

According to equation (4), there are 55 used texture feature number among *{1,2...529}*. Therefore we can compress 529 values to 54 values by removing unused texture feature numbers. By re-labeling we map that these 55 values to the values 0 to 54, i.e., $\{0,1,2,] ,54\}$. In this case, we can define a texture feature number histogram by

$$p_\Delta(n) = \frac{N_\Delta(n)}{N}, n \in \{0,1,2] ,54\} \qquad (5)$$

where Δ is the gray-level variation tolerance given in equation (3), $N_\Delta(n)$ is the frequency of occurrence of the texture feature number n and N is the total number of pixels in the feature image. In Section 2.1, the co-occurrence matrix was defined on gray levels of an image. However, in the TFCM approach we define a co-occurrence matrix on texture feature numbers of the feature image obtained by TFCM, called texture feature number co-occurrence matrix. In analogy with equation (1), a probability distribution of transitions between any pair of arbitrary two texture feature numbers can be defined similarly by

$$p_\Delta(i, j | d_{,r}) = \frac{N_{\Delta, d_{,r}}(i, j)}{N_t}, i, j \in \{0,1,2,] ,54\} \qquad (6)$$

where Δ is the gray-level variation tolerance given in equation (3), $N_{\Delta, d_{,r}}(i, j)$ is defined similarly as in equation (1) with the gray-level variation tolerance Δ, i and j are texture feature numbers rather than gray levels as defined in equation (1) and N_t is the normalization factor which is the total number of *TFN* transitions.

3.3. Texture Feature Descriptors

In this section, we derive 7 texture feature descriptors based on the definitions of equation (5) and (6). The first 4 feature descriptors are derived from the texture feature number histogram given by equation (5) and can be regarded as the zero-th order correlation descriptors since there is no correlation of *TFN*s involved. The 5-th and 6-th descriptors are based on the texture feature number co-occurrence matrix in equation (6), and can be thought of as first-order correlation descriptors because they consider transitions between two *TFN*s. The 7-th descriptor considers the joint occurrence of the TFNs on the same pixels' spatial location *(x, y)* under different gray-level variance tolerance.

1) Coarseness:

$Coarse = \sum_x \sum_y P_\Delta(54)$ where Δ is the specific choice

of the gray-level variation tolerance. A pixel corresponding to *TFN* 41 represents a drastic change in its 8-connectivity neighborhood. So, the total number of these *TFN*s of pixel (x, y) in the feature image also provides a good indication of coarseness.

2) Homogeneity:

$Hom = \sum_x \sum_y P_\Delta(0)$ A pixel corresponding to *TFN* 0

represents no significant change in its 8-connectivity neighborhood. So, the total number of these *TFN*s of pixel (x, y) in the feature image provides a good indication of homogeneity.

3) Mean Convergence:

$MC = \sum\limits_{n=0}^{54} \dfrac{|n \cdot p_\Delta(n) - \bar{}_\Delta|}{\dagger_\Delta}$ where $\bar{}_\Delta$ and $\dagger_\Delta$ are the mean and standard deviation of the TFCM under the Δ. This *MC* feature descriptor indicates how close the texture approximates the mean.

4) Variance:

$Var = \sum\limits_{n=0}^{54}(n - \bar{}_\Delta)^2 \cdot p_\Delta(n)$. The variance measures deviation of *TFN*s from the mean.

5) Code Entropy:

$CE = -\sum\limits_{i=0}^{54}\sum\limits_{j=0}^{54} p_\Delta(i, j | d, \nu)\log p_\Delta(i, j | d, \nu)$ у:

where $p_\Delta(i, j | d, \nu)$ is the (i, j)-th entry of the *TFN* co-occurrence matrix.

6) Code Similarity:

$CS = \sum\limits_{i=1}^{54} p_\Delta^2(i, j | d, \nu)$ where $p_\Delta(i, j | d, \nu)$ is as defined above with $i = j$. This feature descriptor is used to calculate the density of same *TFN*s in its 8-connectivity neighborhood.

7) Resolution Similarity:

$RS = \sum\limits_{x}\sum\limits_{y} \dfrac{P(i, j; x, y)}{1 + (i - j)^2}$. This feature descriptor provides information about the joint probability $p(i, j; x, y)$ of a pixel at (x, y) whose *TFN* is i at $\Delta = 0$ and *TFN* is j at specific Δ. The higher the *RS*, the less the change in *TFN*s of the same pixel, thus, higher RS feature implies the texture is more rough.

4. Experimental Results

In order to evaluate the performance of the proposed method in texture classification, a set of sample images was extracted from Brodatz's natural texture image. 13 sets of natural texture images have been used for this purpose. They are the images of bark, straw, herringbone weave, woolen cloth, pressed calf leather, beach sand, water, raffia, pigskin, brick wall, plastic bubbles shown in Fig. 7. Six texture images of each set under different rotation, each of resolution 256×256 pixels with 256 gray levels were extracted from each Brodatz's texture image. Then each image was divided into 16 sub-images, each of resolution 64×64 pixels. 16 sub-images from the image with rotation 0° were taken as the training samples, whereas the 80 sub-images of the other images were selected as the test samples for classification. In experiments, the tolerance of variation Δ is selected as 3. Figure 8 shows sample images with different rotation and their corresponding TFN histograms of TFCM method and texture spectrums of TS method.

4.1 Classification using the TFN histogram

To demonstrate the discrimination performance of the TFN histogram, we use a supervised classification with the minimum distance rule to classify nature images. The procedure of our experiment is described as follows:

Step 1. When the supervised texture classification algorithm is applied, we select 64 sample images to train the TFN histogram.

Step 2. For each texture type *k*, calculate the TFN histogram of the corresponding training samples and denote it as $\mathbf{S_k}$=S$_k$(j), *k=0,1,...,13* and *j=0,1,...,54.*

Step 3. Calculate the TFN histogram for each considered test sub-images and denote it as **T, T**=T(j)**.**

Step 4. Calculate the distance of TFN histogram between the considered test sub-image and all the training result $\mathbf{S_k}$ as

$$D(T, S_k) = \sum\limits_{0}^{54}|T(j) - S_k(j)| \qquad (7)$$

Step5. The test sub-image will be assigned to class i if the D(T, S$_i$) is the minimum among all classes.

The experimental result listed in Table 1 shows 98.94% average accuracy rate. Similar experiments are also taken in by using the texture spectrum of TS method. The classification results listed in Table 2.

Its correct classification rate only reaches to 62.4%. The experimental results reveal that the TFCM method effectively captures the rotation effects on real texture images than the TS method. Furthermore, the TFCM is nearly rotation invariant.

4.2 Texture classification with the texture features

The features from the TFCM, GLCM and TS were calculated over each sample sub-images of all the thirty texture image classes of Fig. 7. Among the 28 textural features used in classifying Brodatz's texture image, seven were TFCM feature, 13 were GLCM features and remaining eight were TS features. These textural features were compared using a common statistical classification technique. Bayesian minimum risk classifier was used for this purpose. In the Bayesian classifier, the random sample x is assigned to each class i based on the minimum loss rule. A multivariate Gaussian probability density function was assumed for the Bayesian classifier, with each density specified by the mean vector and covariance matrix. The minimum loss was computed by maximizing the decision function

$$d_i(x) = \ln P(w_i) - \frac{1}{2}[(x - m_i)^T C_i^{-1}(x - m_i)] - \frac{1}{2}\ln|C_i| \quad (8)$$

where $d_i(x)$ is the decision function for class i, x the sample feature vector, C_i the covariance matrix, m_i the mean feature vector for class i, and $P(w_i)$ the priori probability of occurrence of class w_i. Classification process was carried out in the following way. All the texture features extracted from each method were used for classification and the results were compared. The corresponding classification results by using the Bayesian classification are summarized in Table 3.

Table 3 shows the classification error rate in classifying the thirteen selected Brodatz's texture images with all features from each method. The average error in classifying the thirteen texture sets

from the GLCM in four different directions ranged from 19.2 to 24.8%. The GLCM in the four different directions were summed up and the 13 texture features were calculated to feed as inputs to the Bayesian classifier. These features from the GLCM with an average error of 19.2% do not improve the classification accuracy. The feature from the TS with an average error of 33.1% showed poor performances among the features from the three methods in classifying the Brodatz's texture images. The features from the TFCM performed well in classifying the thirteen texture sets with the lowest classification error compared to the other two methods. Similar to GLCM method to produce the TFN co-occurrence matrices with four different directions, we generate four texture feature sets of the TFCM method and feed to Bayesian classifier for classification. The 5-th and 6-th features of each texture feature set generate from the different co-occurrence matrix, however, the first four and the last texture features are the same among the four texture feature sets. The four textural feature sets from the TFN co-occurrence matrices result average classification error rates from 1.4 to 2.7%. Summed up the four TFN co-occurrence matrices, corresponding to four different directions, to calculate the texture feature set and feed to the classifier for classification. The corresponding classification error rate is 2.9%.

In chronic liver diseases the severity of infected patients may range from healthy carrier to cirrhosis. The conventional diagnostic method for patients with diffuse parenchyma liver diseases depends mainly on needle biopsy of the liver. However, the pathological measurement of these diseases, such as hepatitis and cirrhosis may be severely biased due to sampling error in the biopsy specimen. Furthermore, it is an invasive procedure that may result in morbidity or even

mortality. Therefore, developing a reliable noninvasive clinical method of evaluating histological changes in sonograms will be a major advance in diagnosis and monitoring of chronic liver diseases.

Several characteristics of liver sonography have been used to evaluate diffuse parenchyma liver diseases. These include changes of echotexture, echogenicity, liver surface, inferior edge and diameter of hepatic and cystic vein. However, the measurement of these characteristics was always subjective based on the clinical doctor's observation. The disease changes of the liver from normal to cirrhosis can be reflected to the changes of echotexture in local texture area. Thus, if we can establish correlation between the changes of local texture and liver disease states, using this information will be a great advantage for classification of liver sonography.

In this section we apply the texture feature coding method, co-occurrence matrix method and texture spectrum method for classification the ultrasonic liver images. Fig 9 shows three instances of ultrasonic liver images. The experiments were conducted using 90 test images, which were classified into three liver disease classes. . The 30 training liver sample images, proved by liver biopsy and equally divided into three disease groups that are normal liver, hepatitis and cirrhosis, are used to train these parameters of the *d*-dimensional multivariate Gaussian functions. These images were proven by liver biopsy and equally divided into 3 groups. Five analysis methods were evaluated based using these 90 test images. We first analyze the classification rates of the five methods. Their confusion matrices are listed in Table 4. In Table 5, the rows of the tables represent the correct results proven by biopsy and the columns of tables are classification resulting from the classification techniques compared. The results show that the result using the texture feature coding method is better

than the other two.

5. Conclusion

A new texture analysis method called texture feature coding method (TFCM) has been developed and tested. The performance of this method has been compared with GLCM and TS by testing some Brodatz's natural texture images. The experimental results reveal that the TFCM is nearly rotation invariant and shows better performance than the GLCM and TS. The classification error with TFCM, GLCM and TS were 2.9%, 19.2% and 33.1%. Extensive studies should be carried out to test the performance of the TFCM in applications such as remote sensing, biomedical and color images, etc.

Reference

[1]**Zucker SW:** Toward a model of texture, Comput. Vision Graphics Image Process, 5: 190-212, 1976.

[2] **Haralick RM, Shanugan K, Dinstein I:** Texture features for image classification. *IEEE Trans. Syst. Man. Cybernet,.* 3: 610-21, 1973.

[3] **He DC, Wang L:** Texture features based on texture spectrum. *Pattern Recognition*, 24: 391-99, 1991.

[4] **Pudil P, Novovicova J, Kittler J:** Floating search methods in feature selection. *Pattern Recognition Letters*, 15:1119-25, 1994.

[5] **Duerinckx A, Rosenberg K, Hoefs J, Aufrichting D, Beugrt C, Kanel G, Lottenberg S:** In *vivio* acoustic attention in liver correlation with blood tests and histology. *Ultrasound in Med. and Biol.*, 14:405-13, 1988.

[6] **Sun YN, Chiu HT, Lin XZ:** A computer system for the analysis of liver cirrhosis from ultrasonic images. *Chinese Journal of Medical and Biological Engineering*, 11:119-35, 1991.

[4] **Wu CM, Chen YC, Hsieh KS:** Texture feature for classification of ultrasonic liver images. *IEEE Trans. Med. Imaging*, 11:141-52, 1992.

[7] **Insana MF, Wagner RF:** Analysis of ultrasound image texture via generalized Richian statistics. *Optical Engineering,* 25:743-48. 1986.

[8] **Insana MF, Wagner RF, Garra BS, Momenan R, Shawker TH:** Pattern recognition methods for optimizing multivariate tissue signatures in diagnostic ultrasound. *Ultrason. Imaging,* 8:165-80, 1986.
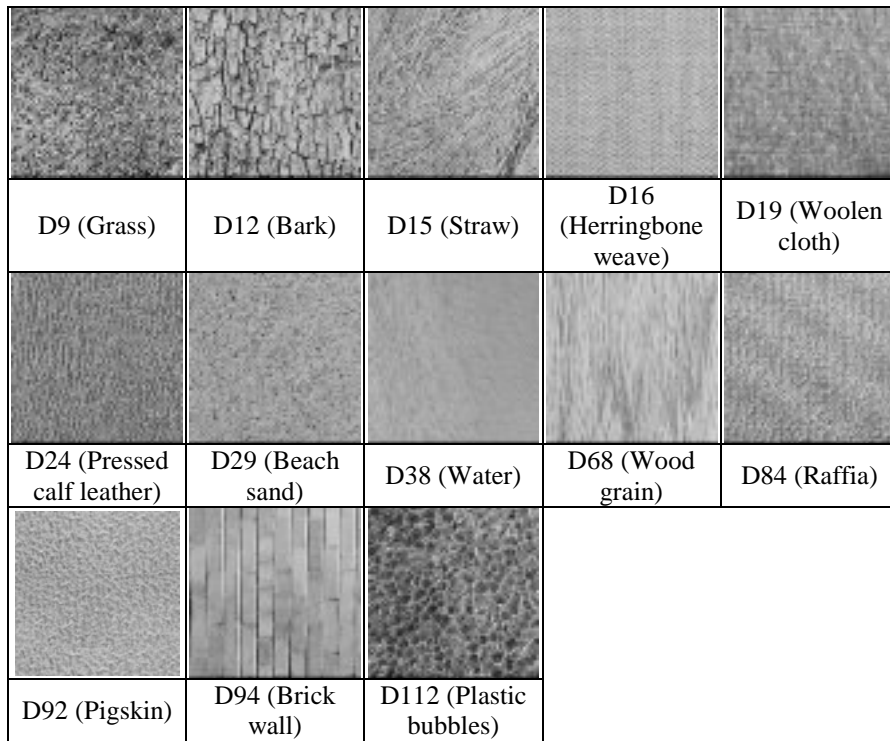
Fig.7. 13 texture images extracted from Brodatz's Album

Table 1. The results of test set classified by using TFN histogram method. In Table 1, the rows of the tables represent the correct texture cluster and the columns of tables are classification resulting from TFN histogram. The correct classification rate is 98.94%.

	D9	D12	D15	D16	D19	D24	D29	D38	D68	D84	D92	D94	D112
D9	80		5										
D12		80											
D15			75										
D16				80				1					
D19					80					2			
D24						80							
D29							80						
D38								80	3				
D68									77				
D84										78			
D92											80		
D94												80	
D112													80

Table 2. The results of test rotational texture set classified by using TS spectrum. In Table2, the rows of the tables represent the correct texture cluster and the columns of tables are classification resulting from TS spectrum. The correct classification rate is 62.40%.
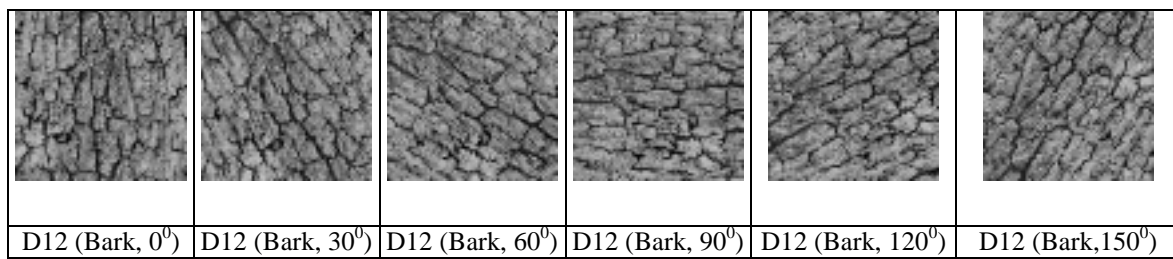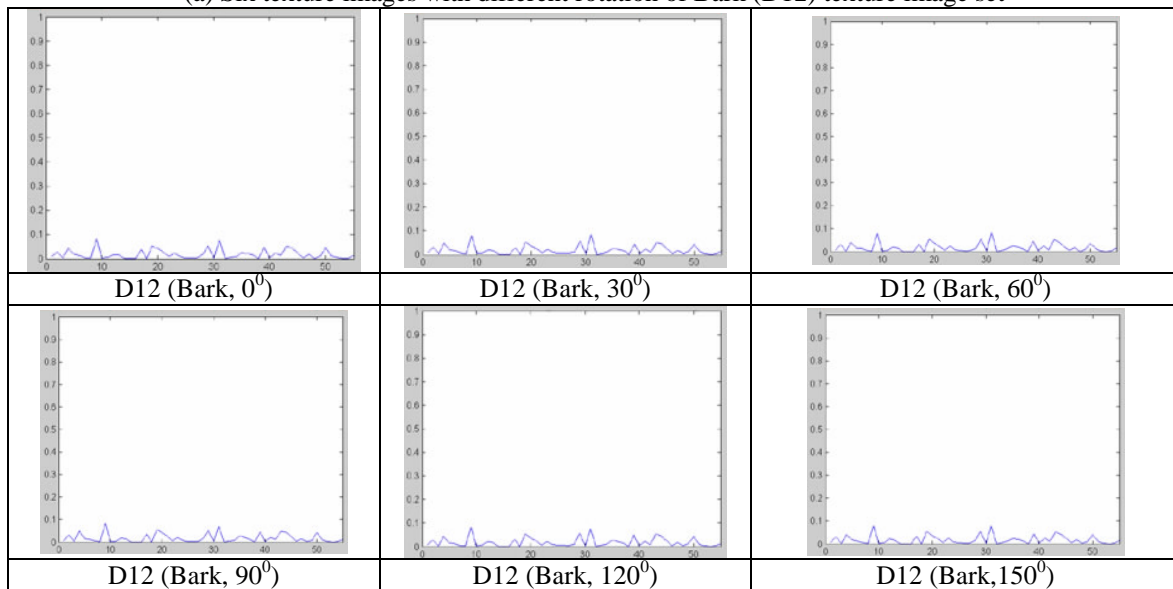
	D9	D12	D15	D16	D19	D24	D29	D38	D68	D84	D92	D94	D112
D9	54									15			12
D12		41										15	
D15			41						14		3		
D16				44		8	11					11	3
D19		12			39				10	9			
D24					14	62							
D29	12						60				14	2	9
D38		2		16				62					
D68			15						46				
D84		10	10	15	16	8			10	56		6	11
D92	14				11	10	12	7			53		
D94		11	14	5								46	
D112													45

Table 3. The classification error rates are computed with all features from the three methods. The displacement of GLCM and TFCM is selected as one pixel.
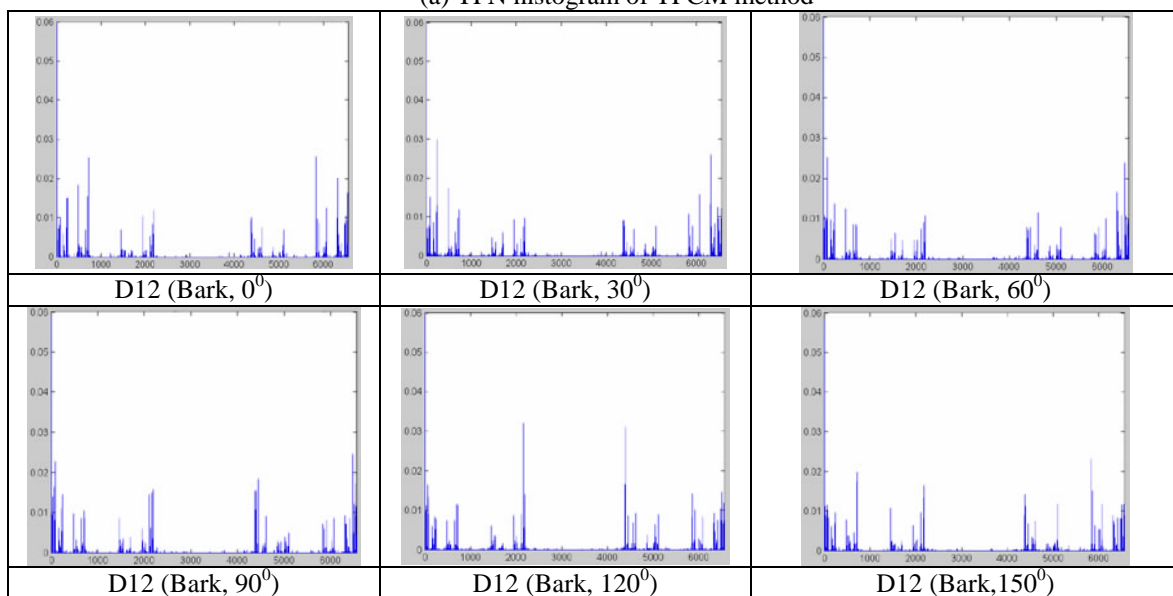
		Texture image class													Average Error (%)
		D9	D12	D15	D16	D19	D24	D29	D38	D68	D84	D92	D94	D112	
Method	Features	Classification error (%)													
GLCM															
0°	1-13	21	26	13	33	22	26	30	18	38	25	19	32	26	23.8
45°	1-13	24	24	16	22	22	23	34	11	22	10	27	34	29	22.9
90°	1-13	36	30	20	19	24	19	36	10	11	22	21	42	33	24.8
135°	1-13	23	22	14	29	18	22	32	9	22	23	17	33	22	20.5
Total	1-13	26	19	17	19	25	21	12	11	17	19	23	22	19	19.2
TS	1-8	38	45	48	31	24	32	39	33	24	25	29	29	34	33.1
TFCM															
0°	1-7	1	0	0	0	3	2	2	1	3	0	2	0	4	1.4
45°	1-7	3	0	1	0	2	1	3	2	3	1	2	3	5	2.0
90°	1-7	3	1	2	1	4	3	2	0	4	3	3	3	6	2.7
135°	1-7	4	0	1	1	1	4	0	0	3	2	1	4	5	2.7
Total	1-7	3	0	3	3	3	5	2	2	2	3	2	5	5	2.9

D12 (Bark, 0^0)	D12 (Bark, 30^0)	D12 (Bark, 60^0)	D12 (Bark, 90^0)	D12 (Bark, 120^0)	D12 (Bark,150^0)

(a) Six texture images with different rotation of Bark (D12) texture image set

D12 (Bark, 0^0)	D12 (Bark, 30^0)	D12 (Bark, 60^0)
D12 (Bark, 90^0)	D12 (Bark, 120^0)	D12 (Bark,150^0)

(a) TFN histogram of TFCM method

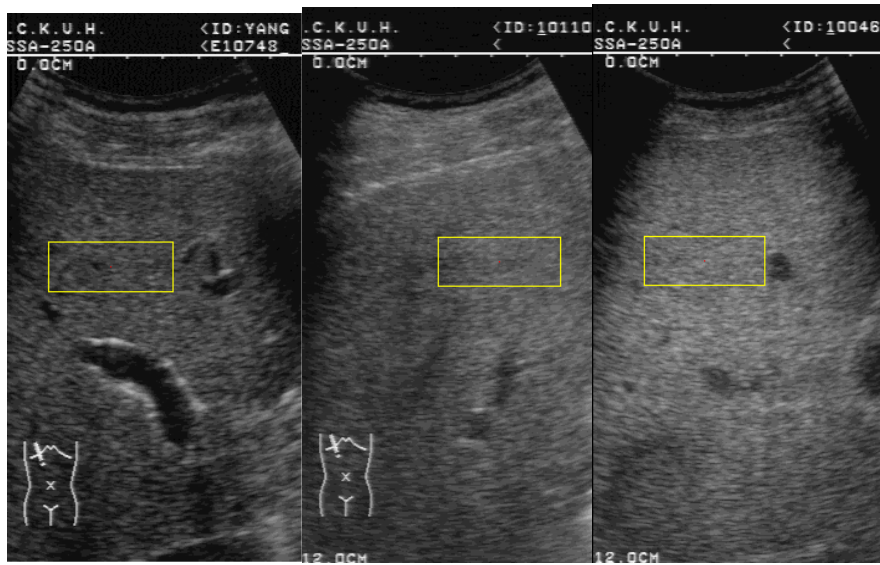|		
D12 (Bark, 0^0)	D12 (Bark, 30^0)	D12 (Bark, 60^0)
D12 (Bark, 90^0)	D12 (Bark, 120^0)	D12 (Bark,150^0)

(b) Texture spectrum of TS method

Fig. 8. Six texture images with different rotation of Bark (D12) texture image set and their corresponding (a) normalized TFN histogram of TFCM method and texture spectrum of TS methods.

13

(a) normal cases   (b)hepatitis case   (c)cirrhosis

Figure 9. Three samples of ultrasonic liver images.   The image (a) is a normal liver.   The images in (b) and (c) are hepatitis and cirrhosis, respectively.

Table 4 Confusion matrices of TFCM, CM and TS.

	Normal	Hepatitis	Cirrhosis
Normal	26	4	0
Hepatitis	3	24	3
Cirrhosis	0	1	29

(a)   Method 1 --- TFCM (texture feature coding method)

	Normal	Hepatitis	Cirrhosis
Normal	22	4	4
Hepatitis	4	20	6
Cirrhosis	0	4	26

(b)   Method 2 – CM (co-occurrence matrix method)

	Normal	Hepatitis	Cirrhosis
Normal	16	8	6
Hepatitis	8	18	4
Cirrhosis	5	7	18

(c)   Method 4—TS (texture spectrum method)

Table 5. Correct classification rates of the five methods evaluated in this paper

Methods	Correcting rates	False-negative rates
TFCM	86.7%	4.4%
CM	75.7%	8.9%
TS	57.78%	12.2%

Accepted and submitted paper about this project

1. **Ming-Huwi Horng, Xiao-Juan Huang and Jia-He Zhuang " Texture Feature Coding Method for Texture Analysis and It's Application" revised in Journal of Optical Engineering, 2001 (SCI).**

2. **MH Horng, YN Sun, XZ Lin and CI Chang "Texture feature coding method for liver sonographic classification", accepted to publication in International Journal of Computerized Medical Imaging and Graphic, 2001 (SCI).**

3. **Ming-Huwi Horng, Xiao-Juan Huang, Jia-He Zhuang and YN Sun "Texture feature Coding Method for texture classification", 2001 CVGIP, Taiwan.**

4. **Ming-Huwi Horng, Xiao-Juan Huang, Jia-He Zhuang "Texture analysis using Texture feature Coding Method", 2001 NCS, Taiwan.**